

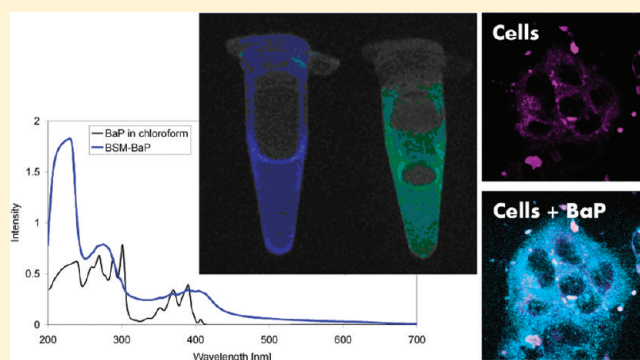
Enhanced Bioavailability of Polyaromatic Hydrocarbons in the Form of Mucin Complexes

Eyal Drug,[†] Dalit Landesman-Milo,[‡] Bogdan Belgorodsky,[†] Natalia Ermakov,[†] Moran Frenkel-Pinter,[†] Ludmila Fadeev,[†] Dan Peer,[‡] and Michael Gozin^{*,†}

[†]School of Chemistry, Raymond and Beverly Sackler Faculty of Exact Sciences, and [‡]Laboratory of Nanomedicine, Department of Cell Research and Immunology, George S. Wise Faculty of Life Sciences and the Center for Nanoscience and Nanotechnology, Tel Aviv University, Tel Aviv 69978, Israel

S Supporting Information

ABSTRACT: Increasing exposure of biological systems to large amounts of polycyclic aromatic hydrocarbons is of great public concern. Organisms have an array of biological defense mechanisms, and it is believed that mucosal gel (which covers the respiratory system, the gastrointestinal tract, etc.) provides an effective chemical shield against a range of toxic materials. However, in this work, we demonstrate, for the first time, that, upon complexation of polyaromatic hydrocarbons with mucins, enhanced bioavailability and, therefore, toxicity are obtained. This work was aimed to demonstrate how complexation of various highly hydrophobic polycyclic aromatic hydrocarbons with representative mucin glycoprotein could lead to the formation of previously undescribed materials, which exhibit increased toxicity versus pristine polycyclic aromatic hydrocarbons. In the present work, we show that a representative mucin glycoprotein, bovine submaxillary mucin, has impressive and unprecedented capabilities of binding and solubilizing water-insoluble materials in physiological solution. The complexes formed between the mucin and a series of polycyclic aromatic hydrocarbons were comprehensively characterized, and their toxicity was evaluated by both *in vivo* and *in vitro* assays. In addition, the bioavailability and membrane-penetration capabilities were tested using an internalization assay. Our results provide, for the first time, evidence of an unknown route by which hydrophobic materials may achieve higher bioavailability, penetrating some of the biological defense systems, in the form of water-soluble complexes with mucosal proteins.



and disposal mechanism for various potentially toxic exogenous materials.^{6,7}

INTRODUCTION

The anthropogenic emission of large amounts of polycyclic aromatic hydrocarbons (PAHs) into the biosphere results from various oil-mining and transportation accidents, as well as the planned combustion of wood, coal, liquid fuels, and domestic and industrial waste.^{1–3} PAHs are well-known as powerful mutagens and carcinogens,^{4,5} and there are many reports regarding an array of biological defense mechanisms, protecting organisms from these materials. For example, it is believed that a mucus (mucosal gel), covering the respiratory and gastrointestinal tracts, should provide an effective physical and chemical shield against a range of toxic materials.^{6,7} The primary components of the mucosal gel are high-molecular-weight mucin glycoproteins that form numerous covalent and noncovalent bonds with other mucin molecules.^{8,9} The condensed and complex nanostructure of the mucus network produces a highly viscoelastic gel that significantly impedes the transport rates of large macromolecules and nanoparticles through it,^{10,11} whereas a high rate of mucosal-gel replacement (a few days in the respiratory system and hours in the gastrointestinal system) offers an effective natural protection

and disposal mechanism for various potentially toxic exogenous materials.^{6,7}

Mucins are large, extracellular glycoproteins with molecular weights ranging from 0.5 to 20 MDa. Cell-membrane-bound mucins and secreted gel-forming mucins share many structural features. Both types of mucins are highly glycosylated, consisting of 80% carbohydrates, primarily *N*-acetylgalactosamine, *N*-acetylglucosamine, fucose, galactose, sialic acid (*N*-acetylneuraminic acid), and traces of mannose. The oligosaccharide moieties of mucins typically exhibit moderate branching and comprise 5–15 sugar monomers. These oligosaccharides are arranged in a “bottle brush” configuration around the polypeptide core of the mucin with the use of *O*-glycosidic bonds to the hydroxyl groups of serine and threonine amino acids of the core. The polypeptide core of the mucin makes up the remaining 20% of the molecular mass (200–500 kDa) of the protein, arranged into distinct regions.⁸

The present study was focused on exploration of the effect of benzo[*a*]pyrene (BaP) on the viability of *Paramecium caudatum*

Received: August 1, 2010

Published: February 18, 2011

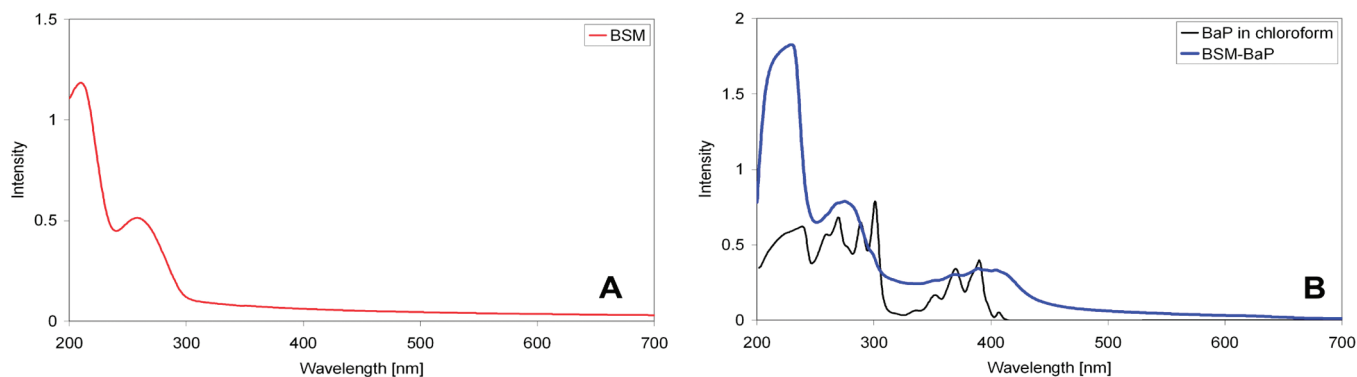


Figure 1. UV-vis spectra of BSM, BaP, and the BaP-BSM complex: (A) BSM in sodium phosphate buffer and (B) BaP in CHCl_3 (blue) and the BaP-BSM complex in sodium phosphate buffer (black).

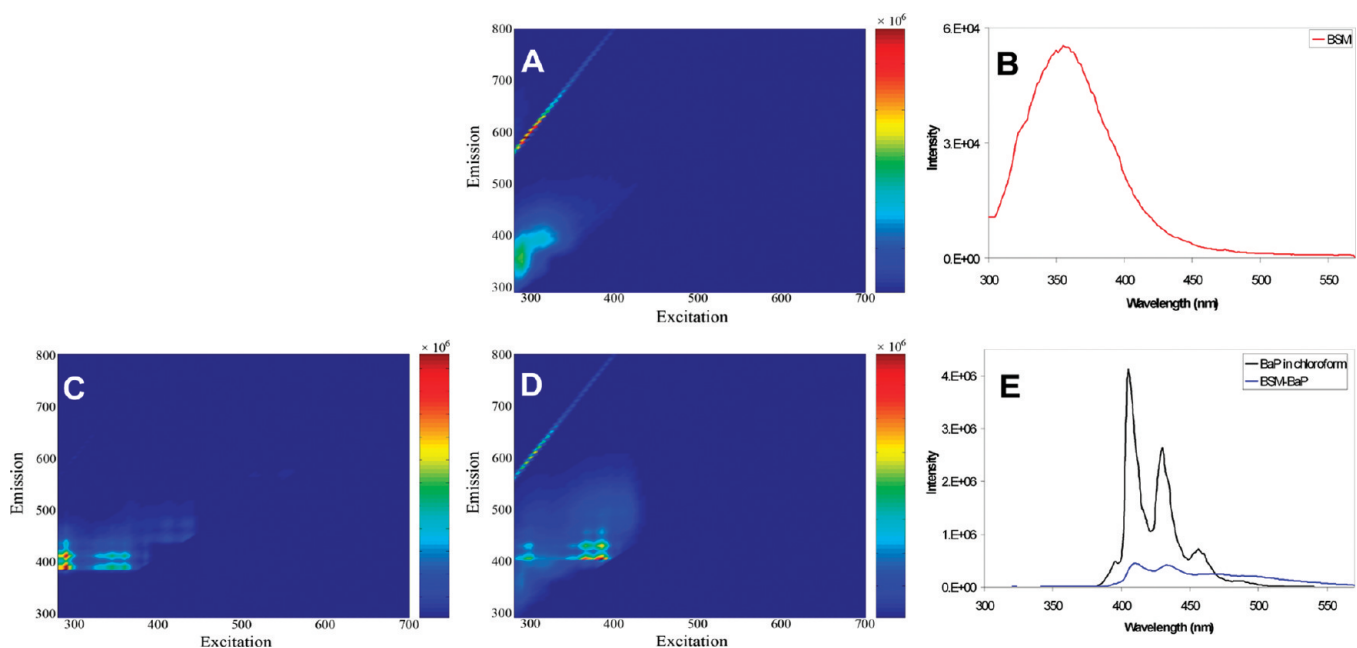


Figure 2. Two- and three-dimensional fluorescence spectra of BSM, ligands, and complexes: (A) three-dimensional spectrum of BSM in sodium phosphate buffer, (B) two-dimensional spectrum of BSM in sodium phosphate buffer, (C) three-dimensional spectrum of BaP in CHCl_3 , (D) three-dimensional spectrum of the BaP-BSM complex in sodium phosphate buffer, and (E) two-dimensional spectra of BaP in CHCl_3 (black) and the BaP-BSM complex in sodium phosphate buffer (blue).

(*in vivo* assay) and Caco-2 cells (*in vitro* assay) and determining LC_{50} values of BaP in sodium phosphate buffer [with 1% dimethyl sulfoxide (DMSO)] versus the BaP complex with bovine submaxillary mucin (BSM) dissolved in the same buffer.

The *in vivo* model, *P. caudatum* (protozoan organism), is widely used to study the biological activity of various organic compounds, including drugs, PAHs,¹² pesticides,^{13–15} and nanoparticles.¹⁶

The *in vitro* model, on the basis of cell proliferation and viability, is a colorimetric assay in which tetrazolium salts (XTT) are used. The assay is based on the cleavage of the yellow tetrazolium salt XTT, by metabolically active cells, to form an orange formazan dye. This cleavage process takes place only in viable cells, and as the number of the living cells increases, the overall activity of mitochondrial dehydrogenases in the sample increases as well. This increase is directly correlated to the amount of dye formed, the concentration of which is monitored by changes in the ultraviolet-visible (UV-vis) absorbance of the samples [enzyme-linked immunosorbent assay (ELISA)

plate reader]. The Caco-2 monolayer assay is widely used in the pharmaceutical industry as an *in vitro* model of the human small-intestinal mucosa, to predict the absorption of orally administered drugs and toxins.^{17,18} Recently,¹⁹ the Caco-2 cell assay was used to demonstrate the toxicity of various benzopyrene isomers. It was found that, when applied in DMSO, only high concentrations of BaP (50 μM) damaged the Caco-2 cells, probably as a result of the low solubility and, therefore, low bioavailability of the BaP.

■ MATERIALS AND METHODS

Materials and Mucin Purification. Prior to incubation of PAH ligands (including anthracene, BaP, and coronene) with BSM type I (Sigma-Aldrich), the glycoprotein was dialyzed overnight against deionized water, with the use of a Spectra/Por Float-A-Lyzer membrane (with a molecular weight cutoff of 100 kDa). Other fine chemicals and solvents of analytical grade were purchased from Sigma-Aldrich.

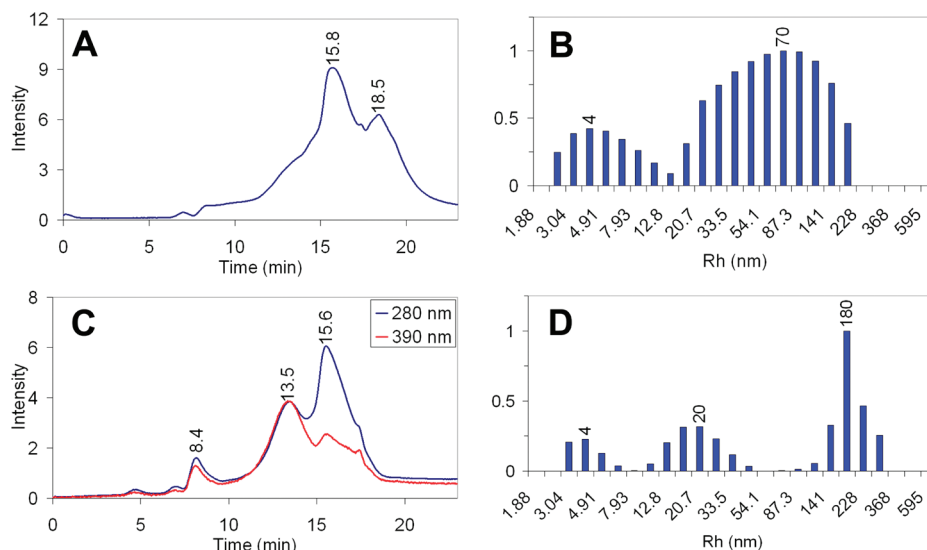


Figure 3. Size-exclusion chromatograms and dynamic-light-scattering analyses of BSM and the BaP–BSM complex: (A) SEC of BSM, (B) DLS of BSM, (C) SEC of the BaP–BSM complex, and (D) DLS of the BaP–BSM complex.

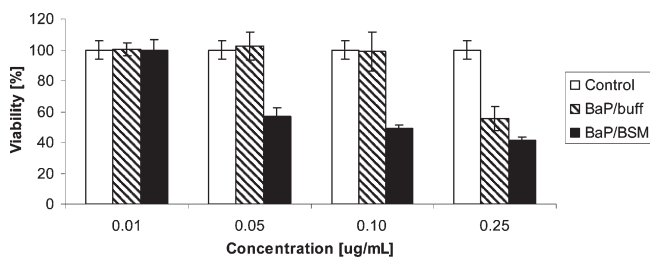


Figure 4. *P. caudatum* assay results. The presented concentrations are of BaP, as calculated from the complex composition. Data are expressed as the mean \pm standard deviation (SD) of four independent experiments, with three repeats per data point in each experiment. $p < 0.05$ (Student's *t* test; refers to the comparison between the “BaP/BSM” samples and the “control” samples in each of the following concentration measurements: 0.05, 0.10, and 0.25 $\mu\text{g}/\text{mL}$). $p < 0.075$ (Student's *t* test; refers to the comparison between the “BaP/Buf” samples and the “control” samples in the 0.10 and 0.25 $\mu\text{g}/\text{mL}$ measurements).

Preparation of Deglycosylated BSM Protein. A solution of 100 mg of BSM protein in 10 mL of 0.1 M NaOH was stirred at room temperature for 30 min, and the resulting solution was cooled to 4 $^{\circ}\text{C}$. To this solution, NaIO_4 was added to a concentration of 100 mM in sodium acetate buffer (100 mM, pH 4.5), and the reaction mixture was stirred overnight at 4 $^{\circ}\text{C}$. Then, 200 mg of glycine was added, and the reaction mixture was allowed to warm to room temperature and stirred for 30 min. After this, 1 mL of 1.0 M NaOH solution was added, and the reaction mixture was stirred for an additional 30 min. The resulting solution was dialyzed overnight against deionized water, then centrifuged, and lyophilized. The degree of BSM deglycosylation was determined by a standard periodic acid/Schiff (PAS) assay (Sigma-Aldrich).

Preparation of Complexes of BSM and Deglycosylated BSM Proteins with PAH Ligands. To a solution of BSM or deglycosylated BSM protein (4 mg/mL, 1.5 mL) in sodium phosphate buffer (2 mM, pH 7.2), a solid PAH ligand (1 mg) was added at room temperature, and the mixture was stirred at 500–700 rpm for 48 h. After this, the reaction mixture was filtered through a 0.45 μm filter, and the solution was loaded on a Sephadex G-25 gel-permeation column (Pharmacia Biotech). PAH–protein complexes were eluted with a sodium phosphate buffer (20 mM, pH 7.2), and their elution was monitored by UV–vis spectroscopy.

Composition of the Mucin Complexes. The amount of BSM or deglycosylated BSM protein in the complexes was determined by a standard PAS assay (Sigma-Aldrich). The amount of PAH ligand in each complex was determined by UV–vis spectroscopy, after protein hydrolysis and quantitative extraction of the ligand by chloroform. To a sample of mucin complex in a sodium phosphate buffer (1 mL, 20 mM, pH 7.2), chloroform (1 mL) and hydrochloric acid (1 mL, 12 M) were added at room temperature. The reaction mixture was sealed in a glass pressure vessel and heated at 80 $^{\circ}\text{C}$ with vigorous stirring for 3 h. After cooling to room temperature, the organic phase containing the extracted ligand was analyzed by UV–vis spectroscopy. The efficiency of the extraction process was verified by analyzing the remaining aqueous phase by UV–vis spectroscopy, to rule out the presence of unextracted ligands.

***P. caudatum* Assay.** The strains of the *P. caudatum* used in this work were obtained from the collection of the Institute of Evolution of Animals of the Polish Academy of Sciences (Czubatinski, Krakow, Poland). The *P. caudatum* culture was grown in sterilized glassware, containing Lozin–Lozinskii medium (pH 7.0–7.7; 0.01% NaCl, 0.001% KCl, 0.001% CaCl_2 , 0.001% MgCl_2 , and 0.002% NaHCO_3), and the organism was fed with bread yeast.^{20,21} Every 10 days, the culture was transferred to a fresh medium and kept at 25 ± 1 $^{\circ}\text{C}$ under constant white-light illumination. Sterile medium was dispersed into glass beakers, and equal amounts of *P. caudatum* culture and yeast were added to each beaker.

The protozoa cultures were exposed to BSM or DMSO (final concentration of 1%) in phosphate buffer solution as control experiments. Toxicity experiments were performed with the use of BaP in DMSO, which was added to phosphate buffer solution (final DMSO content of <1%) or BaP–BSM complex in phosphate buffer solution. The tested cultures were incubated for a period of 72 h. Each experiment consisted of three replicates at four different concentrations (Figure 4). The growth of the *P. caudatum* population and its viability, after exposure to the different examined compounds for 3 days, were determined with the use of a hemocytometer (Hausser Nageotte Bright-Line Counting Chamber) and a microscope. Student's *t* test was applied to assess the significance of the differences between results obtained for each of the experiments.

XTT Assay on the Caco-2 Cell Line. Cell viability was tested on Caco-2, a human colorectal adenocarcinoma cell. These cells were cultured in DMEM-F12, supplemented with 10% fetal calf serum

(FCS), L-glutamine (2 mM), and Pen-Strep solution (1:100; Biological Industries Israel). At 24 h prior to the experiment, the cells were placed onto a 96-well tissue culture plate at a density of approximately 5000 cells per well. On the day of the experiment, the medium was removed and a fresh low-serum medium (2.5%) was added. The cells were subsequently incubated with mucin solution (1.3 mg/mL in 5 mM sodium phosphate buffer at pH 7.2), BaP–BSM complex (in a range of concentrations as described in Figures 5 and 6; the described concentrations are of BaP, after calculating its amount in the complex; reaching the highest BaP concentration of 25 $\mu\text{g}/\text{mL}$), BaP in sodium phosphate buffer (25 $\mu\text{g}/\text{mL}$ of BaP with 1% DMSO, giving the same final concentration of BaP as its concentration in the highest applied dose), or DMSO (1%) in the sodium phosphate buffer for periods of 8 or 72 h. The number of living cells in the treated cultures and untreated control groups was determined using the XTT cell-proliferation assay.²² Student's *t* test was applied to assess the significance of the differences between results obtained for each of the experiments.

Internalization Assay. An internalization assay was performed in a 24-well plate (Cellstar, Greiner bio-one, Frickenhausen, Germany). A total of 10^5 Caco-2 cells (Caco-2 HTB-37 cell line) were seeded on coverslips in DMEM/F12 (HAM) 1:1 medium supplemented with antibiotics (penicillin and streptomycin), L-glutamine, and 5% FCS (Biological Industries, Beit Haemek, Israel).

For membrane staining, the cells were stained using CellTracker DilC18(5)-DS solution (Invitrogen, Carlsbad, CA), diluted 1:5000 with phosphate-buffered saline (PBS).

Cells were exposed to the BaP–BSM complex or BaP solution in 1% DMSO as a co-solvent (in all cases, the final BaP concentration was 2.5 $\mu\text{g}/\text{mL}$, in a volume of 0.5 mL/well) for a period of 1 h at 37 °C in a humidified atmosphere with 5% CO₂. Subsequently, the cells were washed twice using cold PBS, fixated with 4% paraformaldehyde (PFA), and washed again with cold PBS.

The cells were mounted by fluorescent mounting medium (Golden Bridge International, Mukilteo, WA), and fluorescence was measured using the Andor spinning disk confocal microscope and the Meta 510 Zeiss LSM confocal microscope. Laser beams at 390 and 650 nm were used for UV and the CellTracker fluorophore excitation, respectively. Serial optical sections of the cells were recorded for each treatment, and the images were processed using Zeiss LSM Image Browser software. This experiment was repeated twice, and the discussed results are representative.

RESULTS AND DISCUSSION

Preparation and Analysis of Complexes. A series of BSM complexes with anthracene (Ant), BaP, or coronene (Cor) ligands was prepared. The BSM protein was incubated in phosphate buffer solution (at physiological pH) with the selected ligands, introduced as solids into the reaction mixtures. After incubation, the mucin–ligand complexes were separated by filtering through a 0.45 μm filter, followed by open-column gel-permeation chromatography (Sephadex G-25, GE Healthcare). Each of these novel complexes was analyzed by UV–vis and fluorescence spectroscopy, dynamic light scattering (DLS), and size-exclusion high-performance liquid chromatography (SEC). Representative results obtained for the BaP–BSM complex are shown in Figures 1–3. The data for BSM complexes of the other ligands (Ant–BSM and Cor–BSM) are presented in the Supporting Information.

UV–vis and fluorescence spectra measured for all separated PAH–BSM complexes revealed unknown capabilities of this salivary glycoprotein to bring into aqueous solution highly hydrophobic compounds. As shown in Figure 1 and Figure 1S in the Supporting Information (for the case of BaP and other

ligands, respectively), the UV–vis spectra of the obtained complexes showed the superposition of the characteristic BSM peak (at 280 nm), with the absorbance peaks clearly belonging to ligand chromophores. We found that the BSM-complexed Ant, BaP, and Cor chromophores exhibited line-broadening and bathochromic shifts (Figure 1B for BaP, panels B and C of Figure 1S in the Supporting Information for Ant and Cor, respectively, and Table 1S in the Supporting Information) when compared to spectra of the noncomplexed ligands in chloroform. The loss of the fine structure in the spectra of the BSM-complexed BaP and Cor chromophores might indicate that the larger ligands are bound to BSM in the form of π – π stacked dimers or even larger aggregates (Figure 1B and panel C of Figure 1S in the Supporting Information, respectively²³). An additional contribution to this effect could be ascribed to solvophobic interactions, which reduce the vibronic bands of the corresponding spectra. It was previously reported that, upon formation of π – π stacked assemblies, the photochemical properties of an individual molecular component (in this assembly) could be changed.^{24,25} Because aromatic π – π stacking is primarily governed by electrostatic, dispersion, and solvophobic interactions,^{26–30} aromatic chromophores possessing large π -conjugated systems in a polar environment, as in our case, can form π – π stacked assemblies.²³

Complexation modes of the evaluated ligands were further investigated by three-dimensional excitation–emission fluorescence spectroscopy. We found that BSM-complexed Ant, BaP, and Cor exhibited significant decreases in their fluorescence intensities. We observed bathochromic shifts in the maximum emission wavelengths (as compared to fluorescence spectra of noncomplexed ligands in chloroform solution) from 15 nm for Ant (panels C–E of Figure 2S in the Supporting Information) and BaP (panels C–E of Figure 2) to 55 nm for the case in which Cor was used as a ligand (panels F–H of Figure 2S and Table 2S in the Supporting Information). Despite this shift, the fluorescence spectrum of BSM-complexed Ant preserved most of the well-resolved features of the free ligand. In contrast, significant changes were observed in the shapes of the fluorescence spectra of the bound BaP and Cor, relative to the spectra of chloroform solutions of the free ligands. We believe that, in the case of the Cor ligand, the large red shift in the maximum emission of the complexed Cor could not be attributed to solvatochromism alone.³¹ The fluorescence data strongly indicate that discotic Cor ligands are bound to BSM glycoprotein in the form of π – π stacked clusters,^{23,31} supporting our interpretation of the UV–vis spectroscopy results for this ligand.

Further characterization and evaluation of overall sizes of the BSM complexes were performed by DLS and SEC. We found that, in phosphate buffer solution (20 mM, pH 7.2), the native BSM glycoprotein (2 mg/mL) was present in two populations. The SEC chromatogram of the BSM (monitored at 280 nm, Figure 3A) was characterized by two partially overlapping peaks at 18.5 min (smaller entities) and 15.8 min (larger entities). DLS measurements (Figure 3B) indicated that one population comprised species with a median hydrodynamic radius (R_h) of 4 nm, a size that corresponds to the monomeric unit of the BSM protein, with a reported molecular weight of 170 kDa.³² The second population comprised larger species, with a broader range of sizes (R_h of 70 nm), indicating the presence of BSM in the form of oligomers.³³

SEC analysis of BaP–BSM complexation products showed the formation of large-size products (Figure 3E). The chromato-

Table 1. Uptake Abilities of BSM and dBSM, toward the Different PAHs

	Ant	BaP	Cor
uptake by BSM (%)	4.54 ± 0.91	5.35 ± 1.15	7.74 ± 1.55
uptake per BSM monomer (number of ligands)	43 ± 9	36 ± 8	44 ± 9
uptake by dBSM (%)	0.28 ± 0.06	0.23 ± 0.05	0.61 ± 0.12
uptake per dBSM monomer (number of ligands)	2	1	2

gram monitored at 280 nm showed that, although a considerable population of species had the same elution time as the BSM protein (peak at 15.6 min), a significant portion of the material eluted at retention times of 13.5 and 8.4 min. The SEC chromatogram monitored at 390 nm (a wavelength at which only the BaP chromophore is observed) revealed that, although the BaP ligand was present in all species, the host/ligand ratio in larger entities was substantially higher than in species that eluted at 15.6 min. The DLS analysis of BaP–BSM complexation products indicated the presence of two major and one minor population of species (Figure 3D). The lower molecular-weight species, with R_h of 4 nm, were attributed to monomers of BSM, and the larger species, with R_h values of 21 and 179 nm, correspond to BaP–BSM complexation products.

To evaluate our separation/purification protocols, a series of quantification experiments was performed in which the PAH–BSM complexes were quantified before and after separation by gel-permeation chromatography, by the Bio-Rad assay. These quantification experiments showed that about 70% of all injected protein was recovered after the chromatography, clearly indicating that the majority of our protein–ligand complexes are materials suitable for liquid chromatography.

To ascertain the capacity of BSM glycoprotein for various ligands, we determined the amounts of Ant, BaP, and Cor ligands in the corresponding BSM complexes. The amount of BSM protein in each BSM complex was analyzed by a PAS assay.³⁴ To determine the amount of ligand in each complex, we used a hydrolysis-extraction procedure that included heating of the complex in a heterogeneous mixture of hydrochloric acid and chloroform at 80 °C in a sealed vessel and then determining the amount of chloroform-extracted ligand by UV–vis spectroscopy.^{35,36}

We found that the ligand/BSM weight ratio [ligand-uptake percentage (LUP), the weight ratios between the ligand and protein amounts] increased with an increasing molecular weight of the ligand (Table 1). The LUP values were calculated by dividing the amount of extracted ligand by the amount of BSM protein present in the complex. In addition, we calculated the average number of bound ligand (NBL) molecules per BSM monomer by multiplication of the LUP value by the BSM monomer/ligand molecular-weight ratio (eq 1s in the Supporting Information and Table 1). We found that, for all analyzed complexes, the NBL molecules was very similar (with an average of 40 ligands per monomeric unit of BSM). Although surprising, these findings clearly indicate that BSM does not have a strong preference for any of these hydrophobic ligands.

Determining the structural features of mucin responsible for the binding of hydrophobic ligands is a challenging task, because these proteins have amorphous structures. From the heavy glycosylation of the mucin protein backbone, it is reasonable to assume that the oligosaccharide residues are mainly responsible

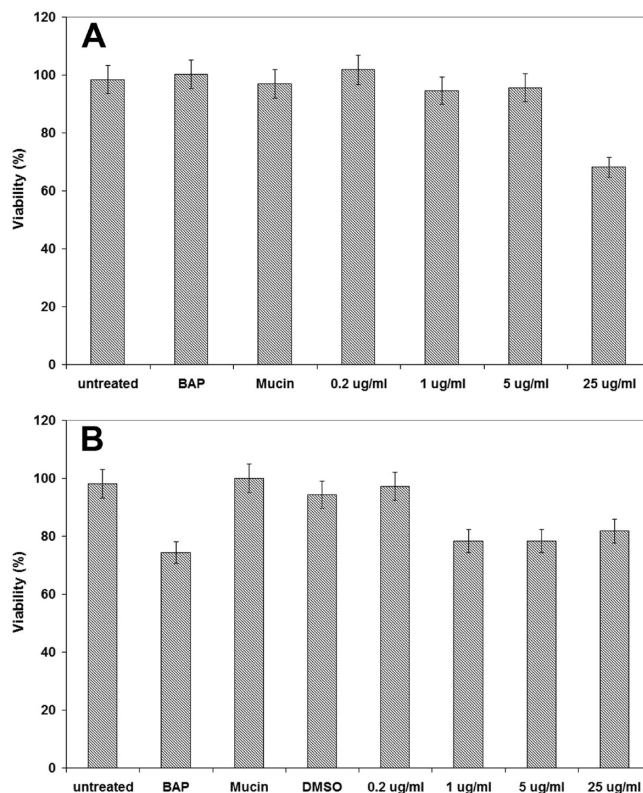


Figure 5. (A) XTT assays results performed on the Caco-2 cell line after 8 h. Data are expressed as the mean ± SD of three independent experiments, with four repeats per data point in each experiment. $p < 0.02$ (Student's t test; refers to the comparison between the 25 $\mu\text{g}/\text{mL}$ measurements or the BAP measurements and the “untreated” bar). $p < 0.06$ (Student's t test; refers to the comparison between the 1 or 5 $\mu\text{g}/\text{mL}$ measurements or the BAP measurements and the “untreated” bar). (B) XTT assays results performed on the Caco-2 cell line after 72 h. Data are expressed as the mean ± SD of three independent experiments, with four repeats per data point in each experiment. $p < 0.02$ (Student's t test; refers to the comparison between the 1, 5, or 25 $\mu\text{g}/\text{mL}$ measurements and the “untreated” bar).

for ligand binding.³⁷ To evaluate this assumption, we prepared a deglycosylated form of BSM (dBSM) and repeated our binding experiments with this protein, as described in the Supporting Information. In a series of binding studies (Table 1), we found that, in comparison to the native BSM protein, the uptake capacity of the dBSM was considerably lower for all tested ligands, clearly demonstrating the key role of the oligosaccharide moieties in the binding of hydrophobic ligands.

Toxicity Assays. In the *P. caudatum* assay, the average cell densities in each examined culture, exposed to the BaP–BSM complex (with a BaP concentration range between 0.01 and 0.25 $\mu\text{g}/\text{mL}$), were measured and compared to the control solutions described above. The results of this assay clearly demonstrated that, while the LD_{50} value for BaP in phosphate buffer is 0.25 $\mu\text{g}/\text{mL}$, this value is significantly lower for the BaP–BSM complex, for which the LD_{50} value was found to be 0.05 $\mu\text{g}/\text{mL}$ (Figure 4). These results clearly express the fact that, upon complexation of the BaP within the matrix of the mucin, higher bioavailability is achieved.

These results were further supported by *in vitro* experiments conducted on a Caco-2 cell line, over two time periods (8 and 72 h exposure), exemplifying acute and chronic exposures. From

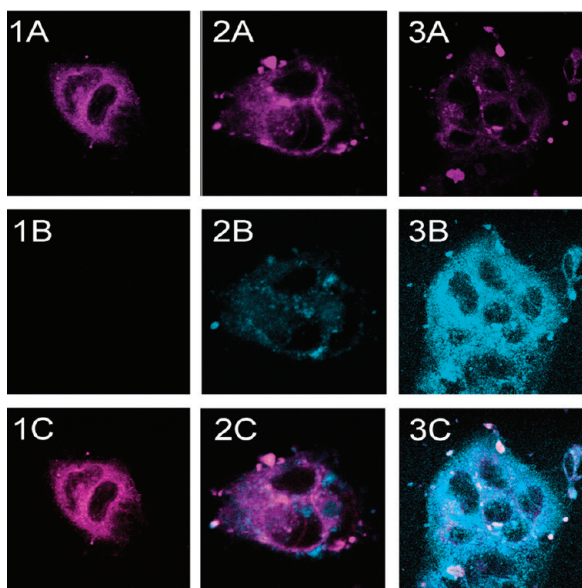


Figure 6. Confocal microscope analysis of Caco-2 cells exposed to the BaP solutions: (1A) fluorescence image of control cells labeled with the membrane dye, analyzed with a 650 nm laser, (1B) fluorescence image of the control cells, analyzed with a 390 nm laser, (1C) computational merging of images 1A and 1B, showing both wavelengths, (2A) fluorescence image of the free BaP-exposed cells, labeled with membrane dye, analyzed with a 650 nm laser, (2B) fluorescence image analysis of the “free” BaP-exposed cells, analyzed with a 390 nm laser, (2C) computational merging of images 2A and 2B, showing both wavelengths, (3A) fluorescence image analysis of the BaP–BSM-exposed cells labeled with membrane dye, analyzed with a 650 nm laser, (3B) fluorescence image analysis of the BaP–BSM-exposed cells, analyzed with a 390 nm laser, and (3C) computational merging of images 3A and 3B, showing both wavelengths.

the results of the 8 h experiment, it was clear that, while the BaP in the phosphate buffer had no toxic effect on the cells, the same concentration of BaP, complexed with mucin, showed a damaging effect on the cells, as their viability dropped to approximately 70% (Figure 5A). Examination of the chronic exposure experiments reveals that, after a period of 72 h, both BaP and the BaP–BSM complex exhibited similar effects of toxicity to the cells, both reducing the viability of the cells to approximately 70% (Figure 5B). From these experiments, we could conclude that, while BaP in its “free” form (dissolved aqueous solution with 1% DMSO) has only chronic effects, the BaP–BSM complex is damaging the cells in an acute manner. Moreover, the fact that, in both experiments, the viability of the cells is similar is giving strength to the conclusion that, upon complexation with BSM, the bioavailability of the BaP is enhanced. In these experiments, control measurements were performed with either mucin solution or 1% DMSO (both in sodium phosphate buffer), and these showed no toxicity to the cells, proving that the source of toxicity is indeed BaP.

To support our hypothesis of the enhanced bioavailability, which is improved by the complexation of the BaP to the mucin, we have performed an internalization assay, in which Caco-2 cells were exposed to BaP in two forms: complexed within BSM (panels 3A–3C in Figure 6) and in its “free” form (panels 2A–2C in Figure 6).

All of the samples, including the control cells, which were not exposed to BaP, and cells which were exposed to the various BaP solutions, were membrane-stained with DilC18 CellTracker dye (panels 1A–3A of Figure 6).

When the intracellular staining is examined (by the BaP fluorophore, $\lambda_{\text{max,ex}}$ at 390 nm), it is clearly shown that the reference cells exhibited no intracellular staining (panel 1B of Figure 6). In contrast, cells that were exposed to the BaP–BSM complex exhibited distinct intracellular staining of BaP (panel 3B of Figure 6). An intense labeling was observed near the nuclei and sparse labeling throughout the cytoplasm. This intracellular staining was dramatically higher than in the case of the cells that were exposed to the DMSO-solubilized BaP (panel 2B of Figure 6). Giving thought to the fact that, in both cases, experimental conditions were identical, it is clear that the BaP bioavailability and membrane penetration are significantly enhanced when BSM is used as a carrier agent.

CONCLUSIONS

In summary, we have shown that a representative mucin glycoprotein, BSM, has impressive capabilities for binding and solubilizing highly hydrophobic materials in physiological solution. Binding experiments with deglycosylated BSM clearly demonstrated the importance of this oligoprotein structure in the complexation/dissolution process of hydrophobic materials. The ability of mucins to solubilize water-insoluble materials suggests that these proteins may function as an active interface of living organisms toward polyaromatic hydrocarbons. *In vivo* and *in vitro* toxicity assays demonstrated for the first time that the mucin-complexation process has profound potential to bring those materials into the cells as well as into living organisms. An internalization assay gave rise to the fact that the enhanced bioavailability is a direct product of using mucin as a carrier agent. When using a mucin, the membrane-penetrating capabilities of the insoluble agent were enhanced, resulting in a better accumulation of the PAH throughout the cytoplasm. We believe that our study contributes to a better understanding of how highly hydrophobic materials can be introduced into living organisms, and on the other hand, further expansion of our work may lead to the development of new drug-delivery or protective systems.

ASSOCIATED CONTENT

Supporting Information. Supplementary analytical methods, analyses of the Ant–BSM and Cor–BSM complexes, and evaluation of the role of glycoside moieties of BSM in the complexation process. This material is available free of charge via the Internet at <http://pubs.acs.org>.

AUTHOR INFORMATION

Corresponding Author

*Fax: +972-3-640-5879. E-mail: cogozin@mgchem.tau.ac.il

Funding Sources

This research was supported by the Nanoscience and Nanotechnology Center of the Tel Aviv University and the Foundation of the Center for Neurologic Diseases at Brigham and Women’s Hospital (Harvard Medical School, Boston, MA).

REFERENCES

- (1) Donaldson, K., Tran, L., Jimenez, L. A., Duffin, R., Newby, D. E., and Mills, N. (2005) Combustion-derived nanoparticles: A review of their toxicology following inhalation exposure. *Part. Fibre Toxicol.* 2, 10.
- (2) Lima, A. L. C., Farrington, J. W., and Reddy, C. M. (2005) Combustion-derived polycyclic aromatic hydrocarbons in the environment—A review. *Environ. Forensics* 6 (2), 109–131.

- (3) Perera, F. P. (1997) Environment and cancer; who are susceptible? *Science* 278 (5340), 1068–1073.
- (4) Luch, A. (2005) Polycyclic aromatic hydrocarbon-induced carcinogenesis—An integrated view, *Carcinogenic Effects of Polycyclic Aromatic Hydrocarbons*, Imperial College Press, London, U.K.
- (5) Poirier, M. C. (2004) Chemical-induced DNA damage and human cancer risk. *Nat. Rev. Cancer* 4 (8), 630–637.
- (6) Holzer, P. (2000) Gastroduodenal mucosal defense. *Curr. Opin. Gastroenterol.* 16 (6), 469–478.
- (7) Lamont, J. T. (1992) Mucus: The front line of intestinal mucosal defense. *Ann. N. Y. Acad. Sci.* 664, 190–201.
- (8) Bansil, R., and Turner, B. S. (2006) Mucin structure, aggregation, physiological functions and biomedical applications. *Curr. Opin. Colloid Interface Sci.* 11 (2 and 3), 164–170.
- (9) Perez-Vilar, J., and Hill, R. L. (1999) The structure and assembly of secreted mucins. *J. Biol. Chem.* 274 (45), 31751–31754.
- (10) Hamman, J. H., Enslin, G. M., and Kotze, A. F. (2005) Oral delivery of peptide drugs: Barriers and developments. *BioDrugs* 19 (3), 165–177.
- (11) Lai, S. K., O'Hanlon, D. E., Harrold, S., Man, S. T., Wang, Y.-Y., and Cone, R. (2007) Rapid transport of large polymeric nanoparticles in fresh undiluted human mucus. *Proc. Natl. Acad. Sci. U.S.A.* 104 (5), 1482–1487.
- (12) Small, M., Epstein, S. S., and Burroughs, M. (1963) The photodynamic effect of the carcinogen, 3,4-benz-pyrene, on *Paramecium caudatum*. *Cancer Res.* 23, 35–44.
- (13) Khovanskikh, A. E., Shemarova, I. V., and Maizel, E. B. (2001) Participation of pyridinecarboxylic acids in endocellular regulation of reproduction in ciliates. *J. Evol. Biochem. Physiol.* 37 (1), 11–18.
- (14) Krest'yaninov, P. A., and Tumanov, A. A. (2002) Current status and prospects of bioassay. *J. Anal. Chem.* 57 (5), 454–470.
- (15) Djebar, M. R., Rouabhi, R., Saci, F. Z., and Berrebah, H. (2009) Toxic effects of combined molecule from novaluron and diflubenzuron on *Paramecium caudatum*. *Am.-Eurasian J. Toxicol. Sci.* 1 (2), 74–80.
- (16) Haneda, K., and Haga, N. (2007) *Paramecium* as a bioassay system for elucidation of cytotoxicity and biocompatibility of nanoparticles: Effects of carbon nanofibers on proliferation and survival. *Jpn. J. Protozool.* 40 (2), 139–146.
- (17) Artursson, P. (1990) Epithelial transport of drugs in cell culture. I: A model for studying the passive diffusion of drugs over intestinal absorptive (Caco-2) cells. *J. Pharm. Sci.* 79 (6), 476–482.
- (18) Schneider, Y. J., Sergeant, T., Ribonnet, L., Kolosova, A., Garsou, S., Schaut, A., De Saeger, S., Van Peteghem, C., Larondelle, Y., and Pussemier, L. (2008) Molecular and cellular effects of food contaminants and secondary plant components and their plausible interactions at the intestinal level. *Food Chem. Toxicol.* 46, 813–841.
- (19) Sugihara, N., Toyama, K., Okamoto, T., Kadowakia, M., Terao, K., and Furuno, K. (2007) Effects of benzo(e)pyrene and benzo(a)pyrene on P-glycoprotein-mediated transport in Caco-2 cell monolayer: A comparative approach. *Toxicol. in Vitro* 21 (5), 827–834.
- (20) Sonneborn, T. M. (1970) Methods in *Paramecium* research, *Methods in Cell Physiology*, Vol. 2, pp 241–339, Academic Press, New York.
- (21) Ershov, Yu. A., Pletneva, T. V., Sinyuk, T. F., and Dolgopolova, V. A. (1999) Evaluation of growth parameters in *Paramecium caudatum* test model for standardization of biological screening. *Bull. Exp. Biol. Med.* 127 (6), 656–659.
- (22) Chan, D. W., Liu, V. W., To, R. M., Chiu, P. M., Lee, W. Y., and Yao, K. M. (2009) Overexpression of FOXG1 contributes to TGF- β resistance through inhibition of p21WAF1/CIP1 expression in ovarian cancer. *Br. J. Cancer* 101 (8), 1433–1443.
- (23) Wu, J., Watson, M. D., Tchebotareva, N., Wang, Z., and Muellen, K. (2004) Oligomers of hexaperihexabenzocoronenes as “super-oligophenylenes”: Synthesis, electronic properties, and self-assembly. *J. Org. Chem.* 69 (24), 8194–8204.
- (24) Kazmaier, P. M., and Hoffmann, R. (1994) A theoretical study of crystallochromy. Quantum interference effects in the spectra of perylene pigments. *J. Am. Chem. Soc.* 116 (21), 9684–9691.
- (25) Pope, M., Swenberg, C. E. (1999) *Electronic Processes in Organic Crystals and Polymers*, Oxford University Press, Oxford, U.K.
- (26) Han, J. J., Shaller, A. D., Wang, W., and Li, A. D. Q. (2008) Architecturally diverse nanostructured foldamers reveal insightful photoinduced single-molecule dynamics. *J. Am. Chem. Soc.* 130 (22), 6974–6982.
- (27) Hunter, C. A., Lawson, K. R., Perkins, J., and Urch, C. J. (2001) Aromatic interactions. *J. Chem. Soc., Perkin Trans. 2* (5), 651–669.
- (28) Rybtchinski, B., Sinks, L. E., and Wasielewski, M. R. (2004) Photoinduced electron transfer in self-assembled dimers of 3-fold symmetric donor–acceptor molecules based on perylene-3,4:9,10-bis-(dicarb-oximide). *J. Phys. Chem. A* 108 (37), 7497–7505.
- (29) Sui, G., Orbulescu, J., Mabrouki, M., Leblanc, R. M., Liu, S., and Gregg, B. A. (2002) Two-dimensional self-assembly of liquid-crystalline perylenediimide derivatives at the air/water interface. *ChemPhysChem* 3 (12), 1041–1044.
- (30) Zhao, D., and Moore, J. S. (2003) Shape-persistent aryleneethynylene macrocycles: Syntheses and supramolecular chemistry. *Chem. Commun.* 7, 807–818.
- (31) Fogel, Y., Kastler, M., Wang, Z., Andrienko, D., Bodwell, G. J., and Muellen, K. (2007) Electron-deficient N-heteroaromatic linkers for the elaboration of large, soluble polycyclic aromatic hydrocarbons and their use in the synthesis of some very large transition metal complexes. *J. Am. Chem. Soc.* 129 (38), 11743–11749.
- (32) Bhavanandan, V. P., and Hegarty, J. D. (1987) Identification of the mucin core protein by cell-free translation of messenger RNA from bovine submaxillary glands. *J. Biol. Chem.* 262 (12), 5913–5917.
- (33) Afdhal, N. H., Niu, N., Nunes, D. P., Bansil, R., Xiang, C. X., and Gantz, D. (1995) Mucin–vesicle interactions in model bile: Evidence for vesicle aggregation and fusion before cholesterol crystal formation. *Hepatology* 22 (3), 856–865.
- (34) He, P., Davis, S. S., and Illum, L. (1998) In vitro evaluation of the mucoadhesive properties of chitosan microspheres. *Int. J. Pharm.* 166 (1), 75–88.
- (35) Downs, F., and Pigman, W. (1969) Destruction of serine and threonine during acid hydrolysis. *Int. J. Protein Res.* 1 (3), 181–184.
- (36) Mantle, M., and Forstner, J. F. (1986) The effects of delipidation on the major antigenic determinant of purified human intestinal mucin. *Biochem. Cell Biol.* 64 (3), 223–228.
- (37) Chen, X., Lee, G. S., Zettl, A., and Bertozzi, C. R. (2004) Biomimetic synthesis: Biomimetic engineering of carbon nanotubes by using cell surface mucin mimics. *Angew. Chem., Int. Ed.* 43 (45), 6111–6116.